

# Light-Induced Metastable Hidden Skyrmion Phase in the Mott Insulator $\text{Cu}_2\text{OSeO}_3$

Benoit Truc, Alexey A. Sapozhnik, Phoebe Tengdin, Emil Viñas Boström, Thomas Schönenberger, Simone Gargiulo, Ivan Madan, Thomas LaGrange, Arnaud Magrez, Claudio Verdozzi, Angel Rubio, Henrik M. Rønnow, and Fabrizio Carbone\*

The discovery of a novel long-lived metastable skyrmion phase in the multiferroic insulator  $\text{Cu}_2\text{OSeO}_3$  visualized with Lorentz transmission electron microscopy for magnetic fields below the equilibrium skyrmion pocket is reported. This phase can be accessed by exciting the sample non-adiabatically with near-infrared femtosecond laser pulses and cannot be reached by any conventional field-cooling protocol, referred as a hidden phase. From the strong wavelength dependence of the photocreation process and via spin-dynamics simulations, the magnetoelastic effect is identified as the most likely photocreation mechanism. This effect results in a transient modification of the magnetic free energy landscape extending the equilibrium skyrmion pocket to lower magnetic fields. The evolution of the photoinduced phase is monitored for over 15 min and no decay is found. Because such a time is much longer than the duration of any transient effect induced by a laser pulse in a material, it is assumed that the newly discovered skyrmion state is stable for practical purposes, thus breaking ground for a novel approach to control magnetic state on demand at ultrafast timescales and drastically reducing heat dissipation relevant for next-generation spintronic devices.

## 1. Introduction


Magnetic skyrmions are topologically non-trivial magnetic textures where the spins twist in a vortex-like fashion around the skyrmion core. Their small size and high speed of current-induced motion make them prospective for various spintronics applications.<sup>[1–5]</sup> Implementing these concepts requires solving multiple fundamental and technological challenges, such as stabilizing room temperature and zero-field skyrmion phases necessary for practical applications in modern information technology. However, in most of the discovered skyrmion-hosting compounds, skyrmions exist only at low temperatures and require external magnetic fields.<sup>[6]</sup> Searching for topologically nontrivial phases at ambient conditions and exploring the ways for their ultrafast manipulation can lead to a different data storage paradigm, allowing for faster data processing without ohmic losses.

B. Truc, A. A. Sapozhnik, P. Tengdin, S. Gargiulo, I. Madan, T. LaGrange, F. Carbone  
Laboratory for Ultrafast Microscopy and Electron Scattering  
Institute of Physics  
École Polytechnique Fédérale de Lausanne  
Lausanne 1015, Switzerland  
E-mail: fabrizio.carbone@epfl.ch  
E. Viñas Boström, A. Rubio  
Max Planck Institute for the Structure and Dynamics of Matter  
22761 Hamburg, Germany

T. Schönenberger, H. M. Rønnow  
Laboratory for Quantum Magnetism  
Institute of Physics  
École Polytechnique Fédérale de Lausanne  
Lausanne 1015, Switzerland  
A. Magrez  
Crystal Growth Facility  
Institute of Physics  
École Polytechnique Fédérale de Lausanne  
Lausanne 1015, Switzerland

C. Verdozzi  
Division of Mathematical Physics and ETSF  
Lund University  
Lund 223 63, Sweden

A. Rubio  
Center for Computational Quantum Physics (CCQ)  
The Flatiron Institute  
New York 10010, USA

 The ORCID identification number(s) for the author(s) of this article can be found under <https://doi.org/10.1002/adma.202304197>

© 2023 The Authors. Advanced Materials published by Wiley-VCH GmbH. This is an open access article under the terms of the Creative Commons Attribution-NonCommercial License, which permits use, distribution and reproduction in any medium, provided the original work is properly cited and is not used for commercial purposes.

DOI: 10.1002/adma.202304197

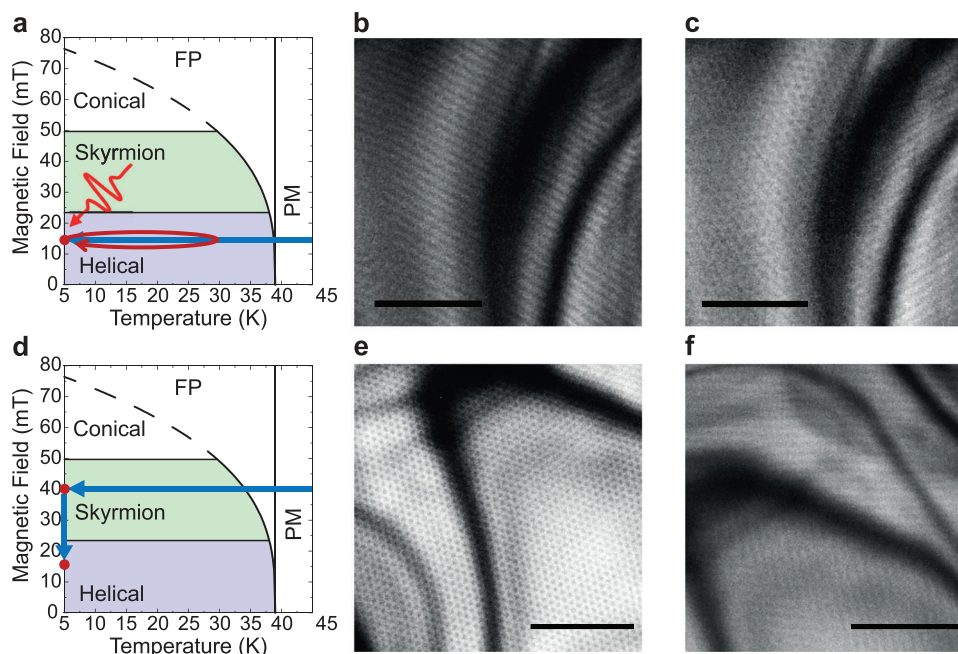


**Figure 1.** New skyrmion phase below the equilibrium skyrmion pocket in  $\text{Cu}_2\text{OSeO}_3$ . a) The field-cooling phase diagram of the  $\text{Cu}_2\text{OSeO}_3$  lamella. "FP" is the field-polarized state, and "PM" denotes the paramagnetic state. b) After field cooling the sample below the equilibrium skyrmion pocket (14 mT), only the helical state is visible in the real-space LTEM image measured at 5 K. c) After the arrival of a single 780 nm laser pulse, the magnetic state of the sample contains coexisting skyrmion and helical phases. d) Protocol followed to attempt accessing the novel skyrmion phase at low magnetic fields by field cooling. e) The skyrmion phase at 5 K and 40 mT generated by field cooling the sample through the Curie temperature. f) After decreasing the magnetic field to 14 mT, the skyrmions disappear, and the helical phase emerges. Scale bars in (b), (c), (e), (f): 1  $\mu\text{m}$ .

Insulating skyrmion hosting compounds are of high interest due to low Gilbert damping,<sup>[7]</sup> which allows for studying the propagation of magnons through a skyrmion crystal<sup>[8,9]</sup> or thermal-gradient-induced skyrmion motion.<sup>[10]</sup> However, such materials are very rare, including multiferroic  $\text{Cu}_2\text{OSeO}_3$ <sup>[11]</sup> and  $\text{Tm}_3\text{Fe}_5\text{O}_{12}$ , where the topological Hall effect was detected at room temperature in Pt/TmIG heterostructures.<sup>[12]</sup>  $\text{Cu}_2\text{OSeO}_3$  is the ideal candidate for studying the light-induced effects due to its bulk Dzyaloshinskii–Moriya interaction (DMI) and a rich phase diagram containing various low-temperature magnetic phases.<sup>[13]</sup> The material exhibits a bandgap of 2.5 eV<sup>[14]</sup> and a local maximum of absorption around 1.5 eV corresponding to the transitions between the 3d levels of Cu split by crystal field effects.<sup>[15]</sup> The equilibrium skyrmion phase in  $\text{Cu}_2\text{OSeO}_3$  can be tuned by an external electric field,<sup>[16,17]</sup> and the electric field-induced creation of skyrmions was recently demonstrated.<sup>[18]</sup> The mechanical strain plays an important role in stabilizing skyrmions in  $\text{Cu}_2\text{OSeO}_3$ , evidenced by a significant expansion of the skyrmion phase at high pressures.<sup>[19]</sup>

Light stimulation provides a fast and versatile way to control the structural and magnetic properties of the materials.<sup>[20]</sup> The coupling between light and the magnetic state of a sample occurs via several mechanisms. These include coupling between the magnetic and the electronic subsystems at an elevated temperature,<sup>[21]</sup> nonlinear phononics,<sup>[22]</sup> a transient magnetic field generated via the inverse Faraday effect,<sup>[23,24]</sup> or the magnetoelastic effect.<sup>[25]</sup> The previous experiments on the photocreation of topological magnetic textures focused on metallic com-

pounds, where the transient heating of the material was identified as the primary microscopic mechanism.<sup>[26–28]</sup>

In this work, we demonstrate the photoinduced creation of skyrmions by a single NIR femtosecond pulse outside the adiabatically accessible regime. We visualized the skyrmions by the Lorentz transmission electron microscopy (LTEM) technique, which provides a high spatial resolution for studying the magnetic materials on the nanoscale.<sup>[29–31]</sup> We successfully generated the skyrmions at low magnetic fields below the equilibrium skyrmion pocket in  $\text{Cu}_2\text{OSeO}_3$  by 780 nm and 1200 nm pulses. Considering the low absorption of  $\text{Cu}_2\text{OSeO}_3$  at 1200 nm, the reported results are relevant for low-power skyrmion-based applications.<sup>[15]</sup>

## 2. Results

The equilibrium phase diagram of the  $\text{Cu}_2\text{OSeO}_3$  lamella was measured by field cooling the sample from 65 K at different magnetic fields and is presented in **Figure 1a**. The cooling rate was  $\approx 1 \text{ K s}^{-1}$ . Field cooling in magnetic fields lower than 24 mT results in the appearance of a helical phase below the ordering temperature  $T_C$ . Magnetic fields exceeding 50 mT correspond to the conical or field polarized (FP) states, which are indistinguishable in the LTEM images. The boundary between these two phases is indicated by a dashed line in **Figure 1a,d**. The measured  $T_C$  of 40 K is lower than the value of 59 K reported earlier.<sup>[11]</sup> This discrepancy might be explained by the difference in the actual sample temperature and the temperature measured by the thermocouple of the sample holder or by the fact that we studied a thin lamella

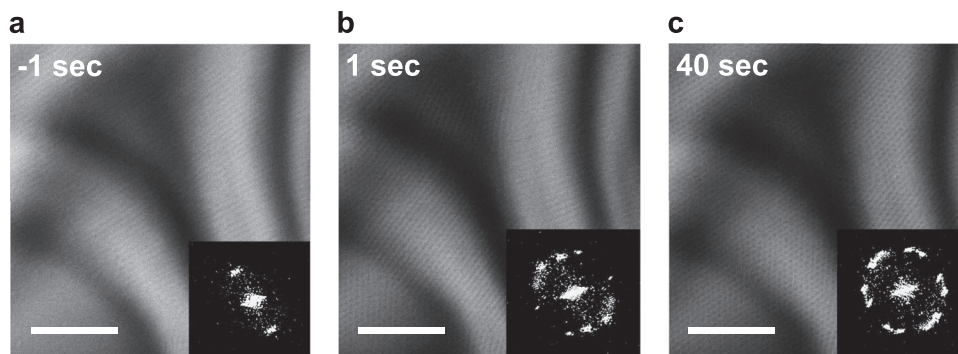


**Figure 2.** The stability of the photocreated skyrmion phase. a–c) The LTEM images of the  $\text{Cu}_2\text{OSeO}_3$  lamella at 5 K and 14 mT one second before (a), one second after (b), and 40 s after (c) the irradiation of the sample by an optical pulse. The insets show the Fourier transform (FT) patterns calculated over the corresponding images. Scale bar is  $1 \mu\text{m}$ .

(150 nm) that may have a different  $T_C$  and phase diagram than the bulk crystal measured in ref. [11].

The skyrmion photocreation experiment below the equilibrium skyrmion pocket was conducted according to the protocol shown in Figure 1a. First, the sample was cooled from 65 K (above the  $T_C$ ) in a field of 14 mT, which is the remanent field of the TEM objective lens, following the blue arrow. The initial state of the sample after field cooling is helical (Figure 1b). After reaching a temperature of 5 K, the sample was irradiated with a single 780 nm femtosecond pulse, resulting in the formation of a skyrmion lattice (Figure 1c). The absorbed fluence in this experiment was  $15 \text{ mJ cm}^{-2}$ .

We tested the possibility of creating the low-field skyrmion phase shown in Figure 1c by slow field cooling. Figure 1d indicates the path followed within the phase diagram. First, the sample is cooled in a field of 40 mT from 65 K to 5 K at a cooling rate of  $\approx 1 \text{ K s}^{-1}$ , resulting in the formation of a skyrmion lattice (Figure 1e). However, after decreasing the magnetic field to 14 mT, the skyrmion lattice transforms into helices (Figure 1f). Thus, the photoinduced skyrmion phase in the  $\text{Cu}_2\text{OSeO}_3$  lamella at 14 mT and 5 K manifests a unique magnetic phase, which can be accessed only via photoexcitation of the sample.

The helical and the skyrmion domains coexist in the sample for a few seconds after the optical excitation, and on a longer time scale, the skyrmion lattice expands prevailing over the helical domains (Figure 2). We followed the evolution of the light-induced skyrmion phase for over 15 min (not shown). During this interval, no evident skyrmion decay was observed. This time is far longer than any residual effect from the laser pulse expected to vanish after few microseconds supported by finite-element simulation as performed in ref. [24]. In addition, the skyrmion phase is stable against the electron beam irradiation.

We studied the pulse duration dependence of the skyrmion photocreation process at 5 K and a field of 14 mT. The final magnetic states of the  $\text{Cu}_2\text{OSeO}_3$  lamella are reported in Figure 3a for the excitation with a single 780 nm pulse. Before each measurement, the sample was reset to a helical state by briefly applying an out-of-plane magnetic field of 1 T. Note that resetting the magnetic state of the sample by field cooling from above the  $T_C$  resulted in an identical initial state. The vertical axis corresponds to the fluence absorbed in the thin 150 nm part of the sample (see Supporting Information). The sample remains in the helical state for lower fluences, as indicated by the black circles. Occasionally, a reorientation of the helix wave vector  $Q$  was observed after the arrival of a pulse, but no skyrmions were created. A skyrmion

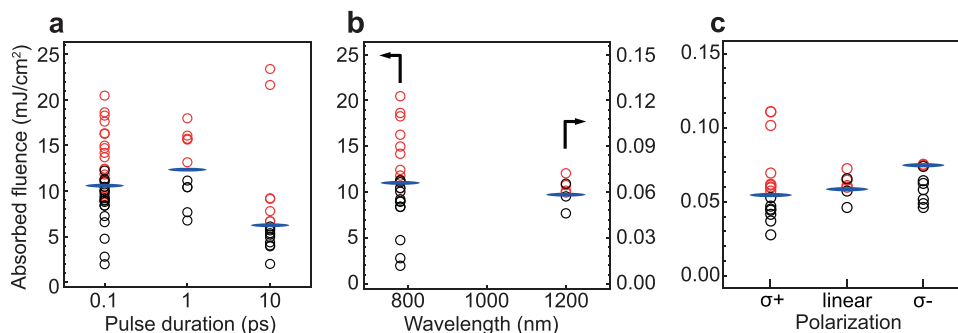


**Figure 3.** Absorbed fluence threshold for the photoinduced generation of skyrmions with NIR photons. a) The pulse duration dependence of the skyrmion photocreation in  $\text{Cu}_2\text{OSeO}_3$  at 5 K and 14 mT for a 780 nm single-pulse photoexcitation. b) Comparison of the photocreation threshold between 780 and 1200 nm optical excitation. c) The photocreation of skyrmions with single femtosecond pulses having a wavelength of 1200 nm for different polarizations. The vertical axis indicates the absorbed fluence. The red and black circles display the final state of the sample exhibiting skyrmions and helices, respectively. The blue horizontal lines indicate the skyrmion generation threshold. The vertical axes in all panels correspond to the absorbed fluence in the thin part of the sample.



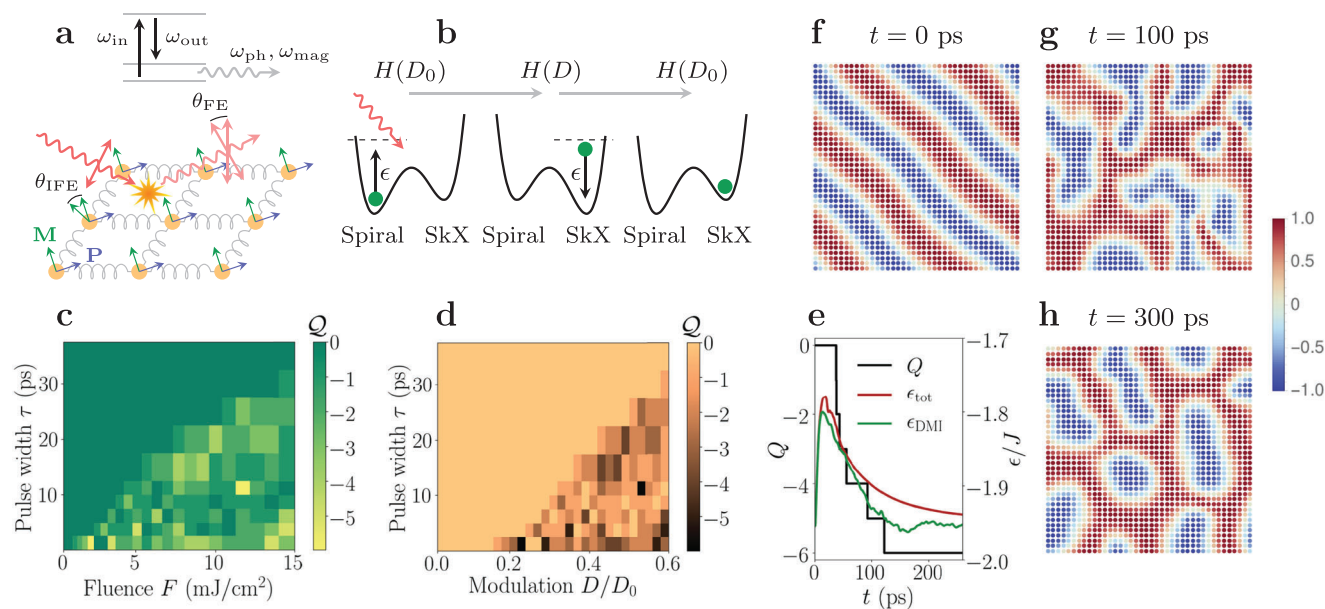


**Figure 4.** Microscopic mechanism of skyrmion photocreation. a) Schematic of the light–matter interaction mechanisms contributing to skyrmion photocreation in  $\text{Cu}_2\text{OSeO}_3$ . Top: Raman scattering processes involving virtual electronic states lead to emission of magnons and phonons. Main: The inverse Faraday effect and a direct magnetoelectric coupling to the polarization (blue arrows) leads to a change in laser polarization and a torque on the magnetic moments (green arrows). b) Heuristic rendering of the mechanism of skyrmion photocreation: 1) Raman and magnetoelectric processes lead to excitation of the coupled spin–phonon system and a change in the free energy landscape. 2) The system relaxes into a quasi-stationary state defined by the photon-modulated Hamiltonian. 3) The system returns to equilibrium trapped in the metastable skyrmion crystal state. c) Non-equilibrium magnetic phase diagram as a function of laser fluence and pulse duration. The areas with a non-zero value of the topological charge  $Q$  correspond to skyrmion photocreation. d) Topological charge  $Q$  as a function of phonon-modulated Dzyaloshinskii–Moriya interaction  $D$ . e) Time-dependence of the topological charge and the total energy per spin during skyrmion creation. f–h) Instantaneous spin configurations at different times  $t$  for the pulse duration  $\tau = 10$  ps and a fluence  $F = 10$  mJ cm $^{-2}$ . The equilibrium spin parameters of the normalized spin model are taken as  $J = 48.2$  meV,  $D = 10.8$ , and  $B = 0.63$  meV (corresponding to  $B = 20.7$  mT), in accordance with the literature. The strength of the light–matter coupling constants are taken as  $g_R = 0.1J$ ,  $g_{\text{FE}} = 0$ ,  $g_{\text{m-el}} = 0.01J$ , and  $g_{\text{m-ph}} = 0.5D$  for a laser electric field of  $E = 10^9$  V m $^{-1}$ .

lattice was generated at higher fluences, corresponding to the red circles. The skyrmion generation threshold marked by the blue lines shows only a weak dependence on the pulse duration.

Tuning the photon energy below the crystal field excitation regime allows for achieving an outstanding efficiency in generating the skyrmions as demonstrated in Figure 3b. The absorbed threshold fluence required for generating the skyrmions with 780 nm pulses at 5 K and 14 mT is 11 mJ cm $^{-2}$ , and for 1200 nm photons, this value reduces to 0.06 mJ cm $^{-2}$ . Although the absolute values vary slightly among the samples tested, we reproduced this result in four different samples. To the best of our knowledge, it is a record-low fluence necessary for generating skyrmions in a magnetic material. The fluence threshold shows only a weak polarization dependence for a wavelength of 1200 nm (Figure 3c). This behavior is expected from the cubic symmetry of the material point group and is consistent with the simulations discussed below.

### 3. Discussion

The low-temperature long-lived metastable skyrmion phase identified in our experiments can only be accessed by laser excitation (Figure 1c) and is absent under adiabatic field cooling of the sample (Figure 1f). It indicates that the photocreation of skyrmions in this regime cannot be explained solely by the transient heating of the sample. Hence, other non-thermal effects must play

a central role. To gain further insight into the microscopic processes underlying skyrmion photocreation in  $\text{Cu}_2\text{OSeO}_3$ , we performed extensive spin-dynamics simulations. Due to the multi-ferroic nature of the material, there is a large number of mechanisms by which the laser electric field can affect the magnetization. Since our measurements were performed at wavelengths inside the bulk bandgap and with low to moderate fluences, real (as opposed to virtual) electronic excitations can be assumed to be negligible. In addition, as indicated by Figure 3b, a much lower fluence is needed to create skyrmions for  $\lambda = 1200$  nm than for  $\lambda = 780$  nm. This is likely due to the electronic crystal field excitations present at shorter wavelengths,<sup>[15]</sup> which hinder energy from reaching the magnetic subsystem and are detrimental to skyrmion creation.

As illustrated in Figure 4a, the possible light–matter coupling mechanisms are the Raman excitation of phonons and magnons, an effective magnetic field generated by the inverse Faraday effect, and direct magnetoelectric coupling to the spontaneous polarization.<sup>[32–34]</sup> The magnetoelectric effect, originating from the coupling between the laser electric field and the electronic polarization of  $\text{Cu}_2\text{OSeO}_3$ , is proportional to the amplitude of the electric field.<sup>[18]</sup> Thus, the fluence threshold is expected to show a strong dependence on the pulse duration and a crystal orientation dependence that we did not observe. In contrast, our experimental data only exhibits a weak dependence of the fluence threshold on the pulse duration (Figure 3a). Thus, the magnetoelectric cou-

pling is likely not the primary mechanism driving the observed photocreation below the equilibrium skyrmion pocket. The inverse Faraday effect is also expected to play a small role in the photocreation process due to the weak polarization dependence for 1200 nm light.<sup>[23]</sup>

In contrast, static mechanical strain is known to modify the shape of the magnetic phase diagram of Cu<sub>2</sub>OSeO<sub>3</sub> and similar materials. An increase of the  $T_C$  and an expansion of the skyrmion pocket were demonstrated in a bulk crystal of Cu<sub>2</sub>OSeO<sub>3</sub> under compressive stress.<sup>[19]</sup> Moreover, a negative uniaxial strain can shift the equilibrium skyrmion pocket to lower magnetic fields via magnetoelastic coupling,<sup>[35]</sup> and mechanical strain can modify the Dzyaloshinskii–Moriya interaction (DMI) constant of a skyrmion hosting compound,<sup>[36]</sup> or both the DMI constant and the anisotropy constant.<sup>[37]</sup> Since a modest strain of 0.3% can induce a modulation of the DMI of up to 20%,<sup>[38,39]</sup> a transient strain mediated by long-wavelength acoustic phonons is expected to have a significant impact on the DMI.<sup>[40]</sup>

To make the above arguments quantitative, we consider a time-dependent light–matter interaction Hamiltonian  $H_I(t)$  accounting for all of the discussed mechanisms. This Hamiltonian is

$$H_I(t) = \sum_{\langle ij \rangle} [J_{ij}(t) \mathbf{m}_i \cdot \mathbf{m}_j + \mathbf{D}_{ij}(t) \cdot (\mathbf{m}_i \times \mathbf{m}_j)] + \sum_i [\mathbf{B}(t) \cdot \mathbf{m}_i - \mathbf{E}(t) \cdot \mathbf{P}_i] \quad (1)$$

where  $J_{ij}$  is the exchange interaction between magnetic moments  $\mathbf{m}_i$  and  $\mathbf{m}_j$ ,  $\mathbf{D}_{ij}$  is the DMI,  $\mathbf{B}$  and  $\mathbf{E}$  are the external magnetic and electric fields, and  $\mathbf{P}_i$  the electronic polarization. Each microscopic process is associated with a characteristic energy scale, denoted by  $g_R$  for the magnon Raman process,  $g_{\text{IFE}}$  for the inverse Faraday effect,  $g_{\text{m-el}}$  for the magnetoelectric coupling, and  $g_{\text{m-ph}}$  for the magneto-phonon coupling. Further, each mechanism mainly affects a single given term in Equation (1), such that the modulation of the exchange depends on  $g_R$ , the DMI on  $g_{\text{m-ph}}$ , the magnetic field on  $g_{\text{IFE}}$  and the polarization on  $g_{\text{m-el}}$ . A detailed discussion of the typical values of these energy scales is provided in the Supporting Information.

To account for the time-dependence of the magnetic interactions, we note that the magnon Raman process, the inverse Faraday effect, and the magnetoelectric effect only modify the spin parameters during the action of the pulse (assumed to be a Gaussian of width  $\tau$ ). In contrast, the phonon modulation of the DMI is expected to persist for as long as there are phonons present in the system. The time-dependent part of the DMI is therefore assumed to have an onset time given by the pulse width  $\tau$  and an exponential decay set by the phonon lifetime  $\tau_{\text{ph}}$ . This time dependence is described by a log-normal function, as further discussed in the Supporting Information.

To describe the skyrmion photocreation process, we simulated the time-evolution governed by Equation (1) following laser excitation (see Supporting Information for a discussion of the equilibrium spin Hamiltonian and phase diagram as well as the spin equations of motion). In line with our experiments, the magnetic field was chosen such that the system is initially in the helical state and close to the phase boundary to the conical state. By exploring a significant portion of the parameter space defined by Equation (1), the dominant mechanism leading to skyrmion

photocreation in Cu<sub>2</sub>OSeO<sub>3</sub> was identified as the transient modulation of the DMI by long-wavelength acoustic phonons. This identification is in line with several previous studies that have found a strong dependence of the Dzyaloshinskii–Moriya interaction (DMI) on strain<sup>[38,39]</sup> as well as on a dynamical coupling to acoustic phonons.<sup>[40]</sup>

In agreement with our experimental results, our simulations predict a skyrmion phase to appear upon laser irradiation for magnetic parameters below the equilibrium skyrmion pocket. Heuristically, the skyrmion photocreation process as emerging from our simulations can be understood as follows (see Figure 4b). The coupled spin–phonon system is excited into a non-equilibrium state through Raman and magnetoelectric processes. Simultaneously, the modulation of the DMI by acoustic phonons leads to a change in the free energy landscape, allowing the system to relax into a quasi-stationary state defined by the instantaneous phonon-modulated Hamiltonian. At a time-scale set by the phonon lifetime  $\tau_{\text{ph}}$ , the free energy landscape returns to its original form, while the magnetic system stays trapped in the metastable skyrmion crystal state.

To substantiate this picture, we show in Figure 4c the non-equilibrium magnetic phase diagram as a function of pulse duration and laser fluence, that illustrates the topological charge  $Q$  of the magnetic state at the final time of our simulations (corresponding to about 300 ps). The topological charge  $Q = 0$  in the helical or ferromagnetic state, and becomes  $Q = -1$  and 1 for skyrmions and antiskyrmions, respectively. Thus the topological charge counts the number of skyrmions and antiskyrmions in the system and is non-zero only when a net imbalance of such excitations exists. Our simulation shows that photoexcitation strongly favors skyrmion creation, and thus  $Q$  in Figure 4c is equal to the total skyrmion number  $N_{\text{sk}}$ . Clearly, above a threshold fluence of  $F \approx 1 \text{ mJ cm}^{-2}$ , the non-equilibrium steady state changes character from a helical to a skyrmion crystal state. Similarly Figure 4d shows the topological charge  $Q$  as a function of DMI modulation.

We note that Figure 4c predicts an approximately linear relation between the threshold fluence and the pulse duration. For this to be consistent with Figure 3a, we have to assume that the spins are insensitive to processes on time scales shorter than about 1 ps. More precisely, assuming that the laser energy is transferred to the acoustic phonons faster than some excitation time  $\tau_{\text{exc}}$ , and that this time is shorter than the characteristic magnetic time-scale  $\tau_{\text{spin}}$ , the resulting spin dynamics is expected to be independent of pulse duration for  $\tau < \tau_{\text{exc}}$ .

To assess the stability of the non-equilibrium skyrmion state, we further investigated the time evolution of the magnetic system. Figure 4f–h shows the instantaneous magnetization  $\mathbf{m}_i(t)$  at a number of different times  $t$ , for a pulse length  $\tau$  leading to a metastable skyrmion state. As seen from Figure 4e, the topological charge changes during the initial part the relaxation process, which is visible in the total energy per spin  $\epsilon_{\text{tot}} = E/N$ . However, after a time  $t = 150 \text{ ps}$ , corresponding roughly to the phonon lifetime  $\tau_{\text{ph}}$ , the topological charge is constant. Within the spin model, the skyrmion state remains stable indefinitely since additional energy would have to be supplied to bring the system back into the helical ground state. This is in good agreement with the experimental finding of a metastable skyrmion state with a long lifetime of at least 15 min.

We finally note that in  $\text{Cu}_2\text{OSeO}_3$ , the equilibrium magnetic phase diagram depends on the orientation of the applied magnetic field due to magnetic anisotropy terms in the free energy.<sup>[13,41,42]</sup> However, in the out-of-equilibrium case studied here, the cubic anisotropy discussed in ref. [38] in Equation (1) does not result in any qualitative differences compared to the isotropic model. This is expected as  $\text{Cu}_2\text{OSeO}_3$  is optically isotropic<sup>[32,43]</sup> and is supported by our experimental results for a  $(1\bar{1}0)$  sample where we did not measure any significant difference in the photocreation threshold in comparison to the (111) samples. For this reason, we have done extensive studies only with the (111) samples, which is the most studied phase and is easy to fabricate due to the preferential growth of the material.

## 4. Conclusion

We have demonstrated the possibility of generating skyrmions in  $\text{Cu}_2\text{OSeO}_3$  at low magnetic fields below the equilibrium skyrmion pocket by NIR femtosecond laser pulses. Supported by the wavelength dependence and spin-dynamics calculations, we claim that the irradiation of the sample results in the triggering of low-energy phonons, which transiently change the DMI. As a consequence, these effects modify the free energy landscape of the material and enable the transformation of the magnetic state into the skyrmion lattice. After 15 min, no decay was observed, which is eight orders of magnitude longer than any laser leftover and robust against electron beam irradiation. Hence, we conclude that the novel reported phase is stable for practical purposes. The threshold fluences for the skyrmion photocreation at 5 K and 14 mT are 11 and  $0.06 \text{ mJ cm}^{-2}$  for 780 and 1200 nm, respectively. The latter is the lowest reported fluence required for generating skyrmions. Thus, our experiment marks a milestone in the development of energy-efficient skyrmion-based spintronics devices.

## 5. Experimental Section

Single crystals of  $\text{Cu}_2\text{OSeO}_3$  were grown by chemical vapor transport in a horizontal two-zone furnace. The precursor for the growth was a stoichiometric mixture of CuO and  $\text{SeO}_2$  sealed in a quartz ampule. The ampule was filled with HCl at a pressure of 100 mbar, acting as the transport agent. A slab of material with a [111] direction normal to it was cut from a  $\text{Cu}_2\text{OSeO}_3$  single crystal and polished to a thickness of 10  $\mu\text{m}$ . A TEM lamella was prepared by further thinning down a  $5 \times 5 \mu\text{m}^2$  to a thickness of approximately 150 nm by Ga ions using the focused ion beam (FIB) technique. The thickness of the sample was determined by electron-energy loss spectroscopy (EELS) log-ratio method.<sup>[44]</sup>

The measurements were performed in a JEOL 2100HR transmission electron microscope (acceleration voltage of 200 kV) equipped with a thermionic gun. The microscope was modified to provide laser light onto the sample.<sup>[45]</sup> The setup was operated at saturation conditions with an electron energy distribution width of 1 eV. The images were recorded on a K2 camera (GATAN) in energy-filtered mode, and the width of the energy-selective slit was set to 10 eV. Magnetic contrast was achieved using Lorentz transmission electron microscopy with an underfocus of 2 mm.<sup>[46]</sup>

A Ti:sapphire regenerative amplifier RAEA HP (KMLabs) produced 35 fs pulses with a bandwidth centered at 780 nm at a repetition rate of 4 kHz. A modified OPA TOPAS (Light Conversion) was utilized for converting them into NIR pulses with a wavelength of 1200 nm. The duration of the 1200 nm pulses was fixed at 100 fs, and that of the 780 nm pulses could be

changed from 100 fs to 10 ps. A set of optical choppers was implemented to reduce the repetition rate to 4 Hz necessary for performing single pump pulse experiments enabled by a fast mechanical shutter.

## Supporting Information

Supporting Information is available from the Wiley Online Library or from the author.

## Acknowledgements

B.T., A.A.S., and P.T. contributed equally to this work. The authors acknowledge support from the ERC consolidator grant ISCQuM No 771346, SNSF via sinergia nanoskyrmionics grant 171003, funding from the European Union's Horizon Europe research and innovation programme under the Marie Skłodowska-Curie grant agreement No 101106809, the Max Planck Institute New York City Center for Non-Equilibrium Quantum Phenomena, the Cluster of Excellence 'CU: Advanced Imaging of Matter' - EXC 2056 - project ID 390715994 and SFB-925 "Light induced dynamics and control of correlated quantum systems" – project 170620586 of the Deutsche Forschungsgemeinschaft (DFG), and Grupos Consolidados (IT1453-22), the Max Planck-New York City Center for Non-Equilibrium Quantum Phenomena, Google Inc., and the Swedish Research Council VR 2022 04486. The Flatiron Institute is a division of the Simons Foundation. The authors would like to gratefully acknowledge Prof. A. Rosch, Dr. N. del Ser, and Prof. J. Zang for helpful discussions and the comments related the theory part of the manuscript.

Open access funding provided by Ecole Polytechnique Federale de Lausanne.

## Conflict of Interest

The authors declare no conflict of interest.

## Data Availability Statement

The data that support the findings of this study are available from the corresponding author upon reasonable request.

## Keywords

femtosecond laser pulses, magnetoelastic effect, multiferroic materials, skyrmions, topological materials, spintronics

Received: May 5, 2023

Published online:

- [1] S. Woo, K. Litzius, B. Krüger, M.-Y. Im, L. Caretta, K. Richter, M. Mann, A. Krone, R. M. Reeve, M. Weigand, P. Agrawal, I. Lemesch, M.-A. Mawass, P. Fischer, M. Kläui, G. S. D. Beach, *Nat. Mater.* **2016**, *15*, 501.
- [2] A. Fert, N. Reyren, V. Cros, *Nat. Rev. Mater.* **2017**, *2*, 17031.
- [3] C. Back, V. Cros, H. Ebert, K. Everschor-Sitte, A. Fert, M. Garst, T. Ma, S. Mankovsky, T. L. Monchesky, M. Mostovoy, N. Nagaosa, S. S. P. Parkin, C. Pfleiderer, N. Reyren, A. Rosch, Y. Taguchi, Y. Tokura, K. von Bergmann, J. Zang, *J. Phys. D: Appl. Phys.* **2020**, *53*, 363001.
- [4] S. Luo, L. You, *APL Mater.* **2021**, *9*, 050901.
- [5] K. Ohara, X. Zhang, Y. Chen, S. Kato, J. Xia, M. Ezawa, O. A. Tretiakov, Z. Hou, Y. Zhou, G. Zhao, J. Yang, X. Liu, *Nano Lett.* **2022**, *22*, 8559.

- [6] Y. Tokura, N. Kanazawa, *Chem. Rev.* **2020**, *121*, 2857.
- [7] I. Stasinopoulos, S. Weichselbaumer, A. Bauer, J. Waizner, H. Berger, S. Maendl, M. Garst, C. Pfeleiderer, D. Grundler, *Appl. Phys. Lett.* **2017**, *111*, 032408.
- [8] C. Schütte, M. Garst, *Phys. Rev. B* **2014**, *90*, 094423.
- [9] J. Iwasaki, A. J. Beekman, N. Nagaosa, *Phys. Rev. B* **2014**, *89*, 064412.
- [10] X. Yu, F. Kagawa, S. Seki, M. Kubota, J. Masell, F. S. Yasin, K. Nakajima, M. Nakamura, M. Kawasaki, N. Nagaosa, Y. Tokura, *Nat. Commun.* **2021**, *12*, 5079.
- [11] S. Seki, X. Z. Yu, S. Ishiwata, Y. Tokura, *Science* **2012**, *336*, 198.
- [12] Q. Shao, Y. Liu, G. Yu, S. K. Kim, X. Che, C. Tang, Q. L. He, Y. Tserkovnyak, J. Shi, K. L. Wang, *Nat. Electron.* **2019**, *2*, 182.
- [13] A. Chacon, L. Heinen, M. Halder, A. Bauer, W. Simeth, S. Mühlbauer, H. Berger, M. Garst, A. Rosch, C. Pfeleiderer, *Nat. Phys.* **2018**, *14*, 936.
- [14] N. Ogawa, S. Seki, Y. Tokura, *Sci. Rep.* **2015**, *5*, 9552.
- [15] R. B. Versteeg, I. Vergara, S. D. Schäfer, D. Bischoff, A. Aqeel, T. T. M. Palstra, M. Grüninger, P. H. M. van Loosdrecht, *Phys. Rev. B* **2016**, *94*, 094409.
- [16] Y. Okamura, F. Kagawa, S. Seki, Y. Tokura, *Nat. Commun.* **2016**, *7*, 12669.
- [17] A. J. Kruchkov, J. S. White, M. Bartkowiak, I. Živković, A. Magrez, H. M. Rønnow, *Sci. Rep.* **2018**, *8*, 10466.
- [18] P. Huang, M. Cantoni, A. Kruchkov, J. Rajeswari, A. Magrez, F. Carbone, H. M. Rønnow, *Nano Lett.* **2018**, *18*, 5167.
- [19] I. Levatić, P. Popčević, V. Šurija, A. Kruchkov, H. Berger, A. Magrez, J. S. White, H. M. Rønnow, I. Živković, *Sci. Rep.* **2016**, *6*, 21347.
- [20] D. N. Basov, R. D. Averitt, D. Hsieh, *Nat. Mater.* **2017**, *16*, 1077.
- [21] B. Koopmans, G. Malinowski, F. D. Longa, D. Steiauf, M. Fähnle, T. Roth, M. Cinchetti, M. Aeschlimann, *Nature Materials* **2009**, *9*, 259.
- [22] D. Afanasiev, J. R. Hortensius, B. A. Ivanov, A. Sasani, E. Bousquet, Y. M. Blanter, R. V. Mikhaylovskiy, A. V. Kimel, A. D. Caviglia, *Nat. Mater.* **2021**, *20*, 607.
- [23] A. V. Kimel, A. Kirilyuk, P. A. Usachev, R. V. Pisarev, A. M. Balbashov, T. Rasing, *Nature* **2005**, *435*, 655.
- [24] P. Tengdin, B. Truc, A. Sapozhnik, L. Kong, N. del Ser, S. Gargiulo, I. Madan, T. Schönenberger, P. R. Baral, P. Che, A. Magrez, D. Grundler, H. M. Rønnow, T. LaGrange, J. Zang, A. Rosch, F. Carbone, *Phys. Rev. X* **2022**, *12*, 041030.
- [25] C. Dornes, Y. Acremann, M. Savoini, M. Kubli, M. J. Neugebauer, E. Abreu, L. Huber, G. Lantz, C. A. F. Vaz, H. Lemke, E. M. Bothschafter, M. Porer, V. Esposito, L. Rettig, M. Buzzi, A. Alberca, Y. W. Windsor, P. Beaud, U. Staub, D. Zhu, S. Song, J. M. Glowia, S. L. Johnson, *Nature* **2019**, *565*, 209.
- [26] M. Finazzi, M. Savoini, A. R. Khorsand, A. Tsukamoto, A. Itoh, L. Duò, A. Kirilyuk, T. Rasing, M. Ezawa, *Phys. Rev. Lett.* **2013**, *110*, 177205.
- [27] G. Berruto, I. Madan, Y. Murooka, G. Vanacore, E. Pomarico, J. Rajeswari, R. Lamb, P. Huang, A. Kruchkov, Y. Togawa, T. LaGrange, D. McGrouther, H. Rønnow, F. Carbone, *Phys. Rev. Lett.* **2018**, *120*, 117201.
- [28] F. Büttner, B. Pfau, M. Böttcher, M. Schneider, G. Mercurio, C. M. Günther, P. Hessing, C. Klose, A. Wittmann, K. Gerlinger, L.-M. Kern, C. Strüber, C. von Korff Schmising, J. Fuchs, D. Engel, A. Churikova, S. Huang, D. Suzuki, I. Lemeshe, M. Huang, L. Caretta, D. Weder, J. H. Gaida, M. Möller, T. R. Harvey, S. Zayko, K. Bagschik, R. Carley, L. Mercadier, J. Schlappa, et al., *Nat. Mater.* **2020**, *20*, 130.
- [29] M. Möller, J. H. Gaida, S. Schäfer, C. Ropers, *Commun. Phys.* **2020**, *3*, 36.
- [30] N. R. da Silva, M. Möller, A. Feist, H. Ulrichs, C. Ropers, S. Schäfer, *Phys. Rev. X* **2018**, *8*, 031052.
- [31] G. Cao, S. Jiang, J. Åkerman, J. Weissenrieder, *Nanoscale* **2021**, *13*, 3746.
- [32] J. H. Yang, Z. L. Li, X. Z. Lu, M.-H. Whangbo, S.-H. Wei, X. G. Gong, H. J. Xiang, *Phys. Rev. Lett.* **2012**, *109*, 107203.
- [33] S. Seki, S. Ishiwata, Y. Tokura, *Phys. Rev. B* **2012**, *86*, 060403.
- [34] Y.-H. Liu, Y.-Q. Li, J. H. Han, *Phys. Rev. B* **2013**, *87*, 100402.
- [35] J. Wang, *Annu. Rev. Mater. Res.* **2019**, *49*, 361.
- [36] Y. Ba, S. Zhuang, Y. Zhang, Y. Wang, Y. Gao, H. Zhou, M. Chen, W. Sun, Q. Liu, G. Chai, J. Ma, Y. Zhang, H. Tian, H. Du, W. Jiang, C. Nan, J.-M. Hu, Y. Zhao, *Nat. Commun.* **2021**, *12*, 322.
- [37] C. Feng, F. Meng, Y. Wang, J. Jiang, N. Mehmood, Y. Cao, X. Lv, F. Yang, L. Wang, Y. Zhao, S. Xie, Z. Hou, W. Mi, Y. Peng, K. Wang, X. Gao, G. Yu, J. Liu, *Adv. Funct. Mater.* **2021**, *31*, 2008715.
- [38] K. Shibata, J. Iwasaki, N. Kanazawa, S. Aizawa, T. Tanigaki, M. Shirai, T. Nakajima, M. Kubota, M. Kawasaki, H. S. Park, D. Shindo, N. Nagaosa, Y. Tokura, *Nat. Nanotechnol.* **2015**, *10*, 589.
- [39] L. Deng, H.-C. Wu, A. P. Litvinchuk, N. F. Q. Yuan, J.-J. Lee, R. Dahal, H. Berger, H.-D. Yang, C.-W. Chu, *Proc. Natl. Acad. Sci. USA* **2020**, *117*, 8783.
- [40] T. Nomura, X.-X. Zhang, S. Zherlitsyn, J. Wosnitza, Y. Tokura, N. Nagaosa, S. Seki, *Phys. Rev. Lett.* **2019**, *122*, 145901.
- [41] F. Qian, L. J. Bannenberg, H. Wilhelm, G. Chaboussant, L. M. Debeer-Schmitt, M. P. Schmidt, A. Aqeel, T. T. M. Palstra, E. Brück, A. J. E. Lefering, C. Pappas, M. Mostovoy, A. O. Leonov, *Sci. Adv.* **2018**, *4*, eaat7323.
- [42] L. J. Bannenberg, H. Wilhelm, R. Cubitt, A. Labh, M. P. Schmidt, E. Lelièvre-Berna, C. Pappas, M. Mostovoy, A. O. Leonov, *npj Quantum Mater.* **2019**, *4*, 11.
- [43] J. H. Yang, Z. L. Li, X. Z. Lu, M.-H. Whangbo, S.-H. Wei, X. G. Gong, H. J. Xiang, *Phys. Rev. Lett.* **2012**, *109*, 107203.
- [44] T. Malis, S. C. Cheng, R. F. Egerton, *J. Electron Microscopy Tech.* **1988**, *8*, 193.
- [45] L. Piazza, D. Masiel, T. LaGrange, B. Reed, B. Barwick, F. Carbone, *Chem. Phys.* **2013**, *423*, 79.
- [46] C. Phatak, A. Petford-Long, M. D. Graef, *Curr. Opin. Solid State Mater. Sci.* **2016**, *20*, 107.